PCCP

PAPER

View Article Online
View Journal | View Issue

Cite this: *Phys. Chem. Chem. Phys.*, 2015, **17**, 422

Enhancing spectral shifts of plasmon-coupled noble metal nanoparticles for sensing applications†

Kristian L. Göeken,[a] Vinod Subramaniam[ab] and Ron Gill*[a]

Received 20th August 2014,
Accepted 5th November 2014

DOI: 10.1039/c4cp03739a

www.rsc.org/pccp

Noble metal nanoparticles possess very large scattering cross-sections, which make them useful as tags in biosensing assays with the potential to detect even single binding events. In this study, we investigated the effects of nanoparticle size on the shift in the light scattering spectrum following formation of Au–Au, Ag–Ag or Ag–Au dimers using FDTD simulations. We discuss the use of a color camera to detect these spectral changes for application in a target-induced dimerization sensing assay. Dimerization of Au nanoparticles induced a larger shift in color compared to Ag nanoparticles. Heterodimers composed of 60 nm Ag and 40 nm Au demonstrated an even larger spectral shift and color response compared to the best homodimer pair (80–40 nm Au). The increased spectral shift of the Ag–Au heterodimer was subsequently observed experimentally for the DNA-induced dimerization of nanoparticles, showing that careful selection of nanoparticle size and composition can significantly enhance recognition of nanoparticle dimerization events for use in (color) sensing assays.

Introduction

Over the past decade there has been a growing need for techniques which are capable of the on-site detection of biomolecules such as DNA/RNA or proteins, to help combat the spread of infectious diseases. Although current diagnostic techniques, such as RT-PCR, are already quite sensitive and specific, they commonly need extensive sample preparation or are time-consuming[1] and expensive,[2] and as such are unsuitable for point-of-care (POC) applications. Localized surface plasmon resonance (LSPR) based nanoparticle (NP) sensors combine high sensitivity with versatility, relative ease of fabrication and readout, making them an attractive option for POC sensing. LSPR sensing is based on detecting shifts in nanoparticle scattering and/or absorption spectra induced by changes in dielectric environment.[3] The technique is generally used to detect changes in bulk solutions or, more locally, (receptor mediated) adsorption of molecules on the nanoparticle surface. Label-free options include using solution-[4] or surface-[5] based particles. However, these are inherently limited in sensitivity due to the minor dielectric changes induced by the small size and low molecular weight of most biologically relevant analytes. Sensitivity can be improved by amplification of the spectral shift. Aggregation-based assays exploit the enhanced redshift caused by large scale plasmonic coupling of nanoparticles in the presence of specific analytes.[6–8] Although such assays are simple in operation and readout, measurable spectral shifts will only occur in the presence of a relatively large amount of aggregation-inducing analytes, which may limit their use in that require high sensitivity applications. Furthermore, ensemble-based detection obscures information concerning binding events at the single particle level. In contrast, observing the spectral shifts of many individual nanoparticles provides additional information and sensitivity. We have recently proposed a sensing concept[9] which offers high sensitivity without the need for time-consuming sample preparations and expensive equipment. The concept is based on detecting the target-induced individual spectral shifts of DNA-functionalized surface-based nanoparticles as they hybridize and plasmonically couple with colloidal nanoparticles. The spectral shifts are detected with a color CCD camera in combination with dark-field microscopy, an approach which is faster and far less complicated than the use of conventional spectrometry. If the spectral shift is sufficiently large, single coupling events may be observed, leading to extremely sensitive and specific detection. Additionally, larger shifts will increase the SNR of color camera based sensing by making it easier to distinguish shifts from fluctuations caused by mere background noise. It will also improve the detection of dimers formed at larger inter-particle distances, which may be of use if long DNA sequences are needed for specificity, or if other larger recognition

[a] *Nanobiophysics, MIRA Institute for Biomedical Technology and Technical Medicine, University of Twente, Enschede, The Netherlands. E-mail: r.gill@utwente.nl*
[b] *FOM Institute AMOLF, Amsterdam, The Netherlands*

† Electronic supplementary information (ESI) available. See DOI: 10.1039/c4cp03739a

elements are used. Finite Difference Time Domain (FDTD) simulations can be used to predict the effects of particle shape, size, dielectric response and inter-particle distance on the LSPR peak[10–13] and can be a useful tool for determining the extent of the spectral shift of nanoparticles upon dimerization. There have been numerous studies investigating the LSPR and refractive index unit (RIU) sensitivity of a wide range of particles such as spheres,[14] triangles,[15] cubes, branches[16] and stars,[17] but only limited attention has been given to optimizing the LSPR shift of plasmon-coupled particles for sensing applications. Martinsson *et al.*[18] investigated the plasmon-coupling of heterogeneous particles separated by dielectric spacers. The study determined that differences in size of the particles in the aggregate can have pronounced effects on the resulting spectral shift. However only ensemble measurements were made, and coupling involved multiple particles, which is not likely to happen in our sensing system at low concentrations of target DNA.

In this paper we describe the results of our FDTD simulations concerning the shift in scattering spectra of surface-based nanospheres upon dimerization with single colloidal nanospheres. Homodimers of gold and silver and their heterodimers are studied to determine which particle combination leads to the largest shift in spectrum and color. These results were then validated experimentally by investigating the target-induced coupling of single nanoparticle pairs for color camera based DNA sensing.

Experimental

FDTD simulations

Simulations were performed using a commercial software package (FDTD Solutions – Lumerical Solutions Inc.). Dielectric constants of gold and silver were fitted to 'CRC Handbook' data points in the software. The mesh size was set to 2 nm. Boundaries were placed at least a wavelength away from each particle to avoid spurious reflections. The angle of incidence was set obliquely to mimic the low contribution of the vertical component of the *P*-polarization in the signal captured by the dark field objective (16°). All simulations were performed in water (n = 1.33), above an infinite silica surface. Coupled NPs were placed next to each other, parallel to the surface and spaced 15 nm apart.

Nanoparticle DNA functionalization

Citrate-coated 40 nm gold nanoparticles (AuNPs) (Nanocomposix) were functionalized using thiolated ssDNA (IBA-lifesciences) by using a modified version of the pH 3 citrate protocol.[19] Briefly, 1 mL of nanoparticles was concentrated to 10 μL by centrifugation (5000*g*, 12 minutes). 20 μL of 100 μM oligonucleotides was reduced by adding 2 μL of 8 mM TCEP (tris(2-carboxyethyl)-phosphine) in 10 mM HEPES 7.4 and incubated for 30 minutes. The reduced DNA was then added to 10 μL of concentrated nanoparticle solution and incubated for 5 minutes. To this solution, 3.6 μL trisodium citrate (pH 3, 100 mM) was added dropwise on a vortex mixer and incubated for 20 minutes. In the next step, 174.4 μL MilliQ water was added. 1 M NaCl was then added in three steps of 30 μL dropwise on a vortex mixer (to reach a final concentration of 0.3 M NaCl), and incubated for 20 min. The solution was then washed using five iterations of centrifugation and resuspension (in 10 mM HEPES buffer pH = 7.4) and stored at 4 °C until used.

Nanoparticle deposition

For the deposition of Ag or AuNPs, glass coverslips were cleaned in hot piranha solution (70% H_2SO_4, 30% H_2O_2) for 30 minutes, hydroxylated by treating the slides with 1 hour of UV/Ozone (Bioforce) and coated by submerging the slides in 1% APTES (3-aminopropyltriethoxysilane) in ethanol for 30 minutes. Slides were then sonicated in MilliQ water for 15 minutes and incubated at 120 °C for at least 15 hours. Citrate-coated NPs were then deposited on the positively charged APTES/glass interface.

Formation of dimers detection assay

Surface-based NPs were functionalized using capture ssDNA (see Table S1, ESI† for DNA sequences). Target DNA was then hybridized to the capture DNA in 10 mM HEPES (pH = 7.4), 0.3 M NaCl, 0.01% sodium dodecyl sulphate. The surface was washed and a true color CCD image of the NPs was made. Finally, tag-functionalized 40 nm AuNPs were allowed to hybridize with the target DNA. The surface was washed again and a second color image was captured.

Data analysis and spectral measurements

For the data analysis, a custom Matlab analysis script was used to overlay the images acquired both before and after hybridization and to determine the color (RGB) change of each individual particle in the image. The changed and unchanged particles were then localized and subsequently spectroscopically analyzed. Spectroscopic measurements were performed on an Ocean Optics QE65000 spectrometer fiber-coupled to an Olympus GX71 dark field microscope. The integration time was 20 s and the spectrum was corrected for the spectrum of the light source. Spectral smoothing was achieved using a 2nd order 100 point Savitzky–Golay window. Bayer color filter arrays (CFA) used were those installed in a Zeiss Axiocam HRc color camera.[20]

Results and discussion

In the proposed sensing scheme, at least two nanospheres are coupled together by target-induced DNA hybridization between the surface bound and the colloidal nanoparticles (Fig. 1a). The hybridization can be followed by detecting the shift in color, induced by the plasmonic coupling of the formed particle complexes (dimers, trimers, *etc.*), with a camera. The number of complexes formed and their respective color shifts are directly related to the concentration of target DNA present. The plasmonic coupling has two main advantages. It results in a much larger spectral shift compared to the binding of DNA alone, and it increases specificity by including two hybridization steps which both need to occur for a signal to be produced.

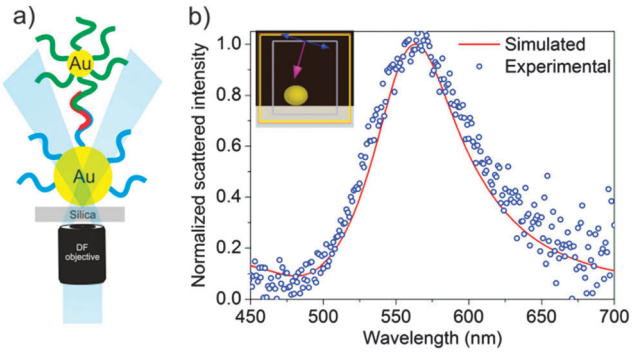

Fig. 1 (a) DNA sensing scheme based on target-induced dimerization of surface-based and colloidal nanoparticles, (b) measured and simulated spectrum of an 80 nm spherical AuNP on glass. Inset: polarization (blue) and *k*-vector (magenta). The white box denotes the total-field scattered-field source. The yellow box denotes the scattering cross section field monitor.

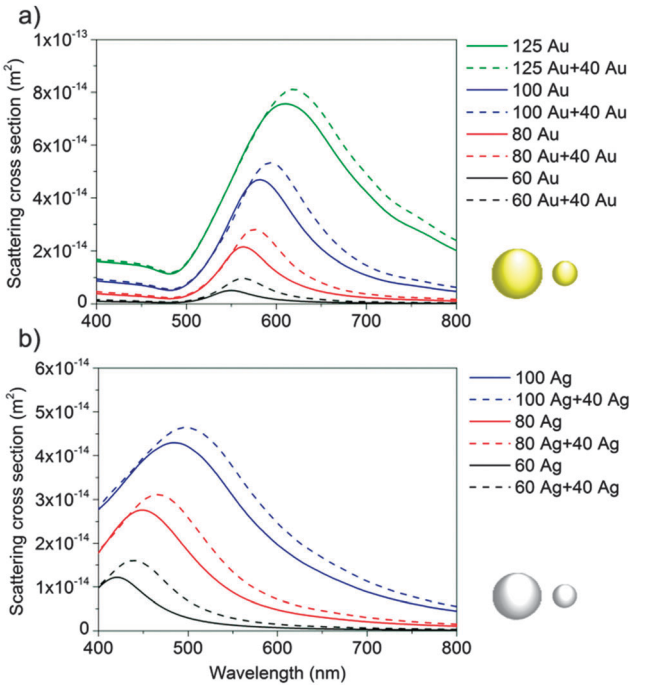

Fig. 2 Simulated scattering spectra of spherical gold (a) and silver (b) nanoparticles in water on glass, with and without a coupled 40 nm AuNP or AgNP.

The colloidal nanoparticles have to be sufficiently large to induce a substantial spectral shift. However, very large particles exhibit stability problems which can lead to aggregation during DNA functionalization. In contrast, the surface-based particles merely need to be large enough to be visible under typical dark-field exposure conditions. We decided to study the coupling of 40 nm NPs as a balance between colloidal stability and spectral response. The most commonly used materials for LSPR sensing are gold and silver, due to convenient positioning of their LSPR peak in the visible region of the spectrum.[21] Gold has high chemical stability, while silver is more sensitive to refractive index changes due to a combination of a higher slope and absolute value of the real part of the dielectric constant of silver compared to that of gold.[22] Small silver particles generally also scatter more light due to the material's low imaginary part of the dielectric constant between 400 and 500 nm, which decreases optical damping.

Before using FDTD to model dimers, the method was first validated by measuring the scattering spectrum of a single 80 nm gold sphere on glass, and plotting it together with the simulated data (Fig. 1b). Both the peak wavelength and the peak width match up well with the FDTD data. Simulations were then used to determine the extent of spectral shifts of different-sized Ag and Au spheres following dimerization with a 40 nm sphere (Fig. 2). The main LSPR peaks of these particles have spectral linewidths which increase with increasing particle diameter. Both gold and silver show a redshift and an increase in scattering cross-section following dimerization. From these graphs it is not apparent which dimer set would be best suited for use in a color camera detection assay, because in contrast to spectroscopic measurements, the sensitivity of color-based measurements also depends on both the position of the resonance peak in relation to the spectral response of the camera as well as the RGB filters used in the CFA. To quantify these spectral shifts and relate them to the sensitivity of the color CCD camera used in our sensing scheme, the Bayer CFA spectra (Fig. S2, ESI†) were multiplied with the simulated spectra of the single and dimer pairs. The spectra were then integrated and the change in each color channel following dimerization is presented as a percentage of the original intensity in that channel. The figure of merit (FOM) is then the sum of the percentages representing the color shifts of all three color channels. The FOM of the spherical dimers is shown in Table 1. The largest optical shift for gold occurs when a 40 nm AuNP binds to a 60 or 80 nm AuNP, induced by the relatively large peak shift compared to the other size-combinations and positioning of the shift near an area of high sensitivity of the CFA. Table 1 shows that although the wavelength shift is higher for silver, the FOM is actually lower. This is due to the

Table 1 Wavelength shift and figure of merit (FOM) of spherical gold and silver homo- and heterodimers

Dimer set	λMax1	λMax2	Δλ	FOM
40Au + 40Au	541	553	12	12
60Au + 40Au	550	563	13	15
80Au + 40Au	563	576	13	15
100Au + 40Au	582	594	12	9
125Au + 40Au	610	620	10	3
60Ag + 40Ag	421	439	18	8
80Ag + 40Ag	449	466	17	9
100Ag + 40Ag	485	497	12	5
40Ag + 40Au	400	546	146	55
60Ag + 40Au	421	548	127	29
80Ag + 40Au	445	550	105	16
100Ag + 40Au	484	557	73	11
60Au + 40Ag	550	403	147	12
80Au + 40Ag	564	402	162	7
100Au + 40Ag	582	400	182	5

unfavorable location of the plasmon peak in a region of low sensitivity of the blue filter in the CFA.

Color- and spectroscopy-based detection of dimerization events can be improved by increasing the LSPR peak-to-peak distance. To that end, we calculated the spectra of gold–silver heterodimers. First, we simulated the binding of large silver particles to 40 nm gold. In this case, two distinct spectral peaks appear (Fig. 3a). The silver LSPR peak (450 nm) is only slightly shifted, but an additional gold peak at around 550 nm appears following dimerization. Although the gold particle is 15 nm from the surface of the silver, and has a plasmon peak shifted about 75 to 100 nm from the silver peak, we find that the Au peak is substantially enhanced compared to the scattering intensity of a single 40 nm Au particle (Fig. 3a, inset). We believe this peak originates from off-resonant coupling between the AgNP LSPR and AuNP LSPR. A similar phenomena was recently described by the Schatz group.[23] Table 1 shows that both the large spectral distance between the two peaks and the apparent order of magnitude enhancement of the scattering cross-section of the AuNP compared to single AuNPs lead to a much higher FOM than for homodimers of silver or gold. Under typical dark field conditions using exposure times of 300 ms, 40 nm gold and silver particles are difficult to detect. However, 60 nm AgNPs have a sufficiently large scattering cross-section and show double the FOM of the best homodimer, indicating that for a typical color camera, coupling between a 60 nm AgNP and a 40 nm AuNP would result in the largest optical shift.

We then investigated the opposite case, namely the binding of large gold particles to 40 nm silver. For these dimers, we only see the appearance of an additional weakly enhanced silver peak at the blue edge of the sensitivity of the CCD (Fig. 3b), which is reflected by the low FOM. We attribute this difference to the high imaginary part of the dielectric constant of gold at wavelengths below 500 nm, where low field enhancements induce only weak plasmon–plasmon coupling.

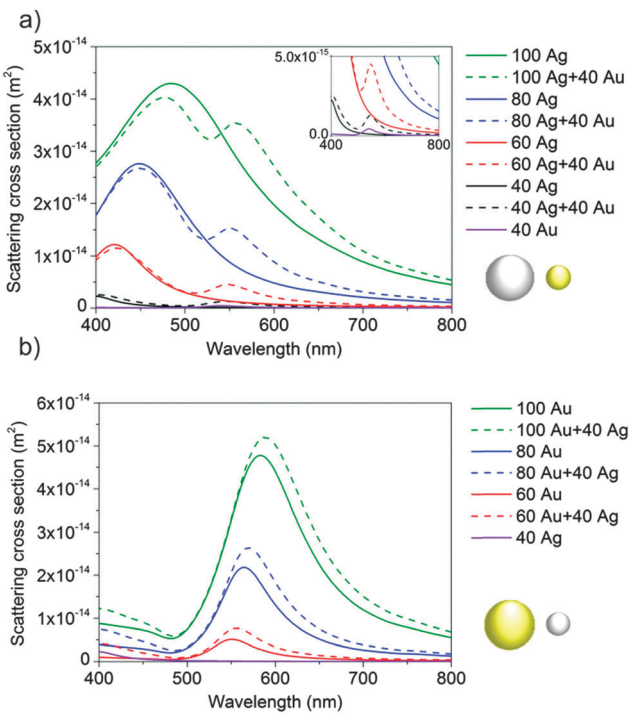

Fig. 3 Simulated scattering spectra of hybrid Ag–Au nanoparticles with varying sizes of (a) silver and (b) gold. Inset in (a) shows magnified spectra.

To validate the simulation data experimentally, dimers were prepared *via* DNA hybridization. Briefly, glass coverslips were coated with a positively charged organosilane layer (APTES). On this layer, negatively charged citrate capped 80 nm Au, 80 nm Ag or 60 nm Ag particles were deposited. The inter-particle distance was controlled by selecting a specific particle concentration and incubation time such that most particles had more than 1 μm spacing and remained singular. These particles were then functionalized with thiolated oligonucleotides which are complementary to part of a target strand. In the next step, the target strand was added at a very low concentration (1E-13M) such that it is unlikely that more than one strand hybridizes to the DNA on each nanoparticle. Finally, colloidal 40 nm gold nanoparticles functionalized with a complementary sequence to a second part of the target strand were allowed to hybridize to the target strand that was bound to the DNA on the particles. To confirm that our method results in the formation of two populations – single particles and dimers, we investigated the influence of the target concentration on the binding of 40 nm AuNPs. SEM images (Fig. S3, ESI†) showed that at 1E-13M target concentration, only a small number of 80 nm AuNPs are bound to a single 40 nm AuNP, while the other 80 nm AuNPs remained unbound. The images also showed non-specific binding of the 40 nm AuNPs to the APTES layer on the glass, but in most cases at distances where plasmon coupling with the AuNPs is very weak or non-existent (>100 nm). The formation of Ag–Au dimers at 1E-13M target concentration was also confirmed for 80 nm Ag and 60 nm Ag (Fig. S4, ESI†).

To determine which particles remained singular, and which particles formed dimers, images were made using a color camera before and after incubation of the 40 nm AuNPs, followed by analysis of the color of each individual particle in the before and after images. The particles which showed no change in color were determined to be singular particles, which was verified by the SEM images and color-change data of the particles in our negative control (no target). Spectroscopic analysis was then performed on the individual particles which showed a color change (dimer) and the particles which showed no change (singular). Fig. 4 shows the spectra of the singular 80Au, 80Ag and 60Ag particles plotted together with the 80Au–40Au homodimers, 80Ag–40Au and 60Ag–40Au heterodimers. For 80Au–40Au, the spectral shift following formation of the dimer is very similar to the simulated data. A small redshift is observed together with an increased width of the plasmon peak. The average peak shift of the measured dimers lies around 19 nm, which is 45% higher than estimated in the simulations. This larger shift might be attributed to smaller particle-to-particle distances caused by movement of the particle to a local charge repulsion minimum due to flexibility of the less rigid 9 adenine single stranded DNA spacer, as well as the nick in between the three DNA strands. From the SEM images it can be observed that the particles seems to prefer attachment close to the positively charged APTES layer on the glass. This would then

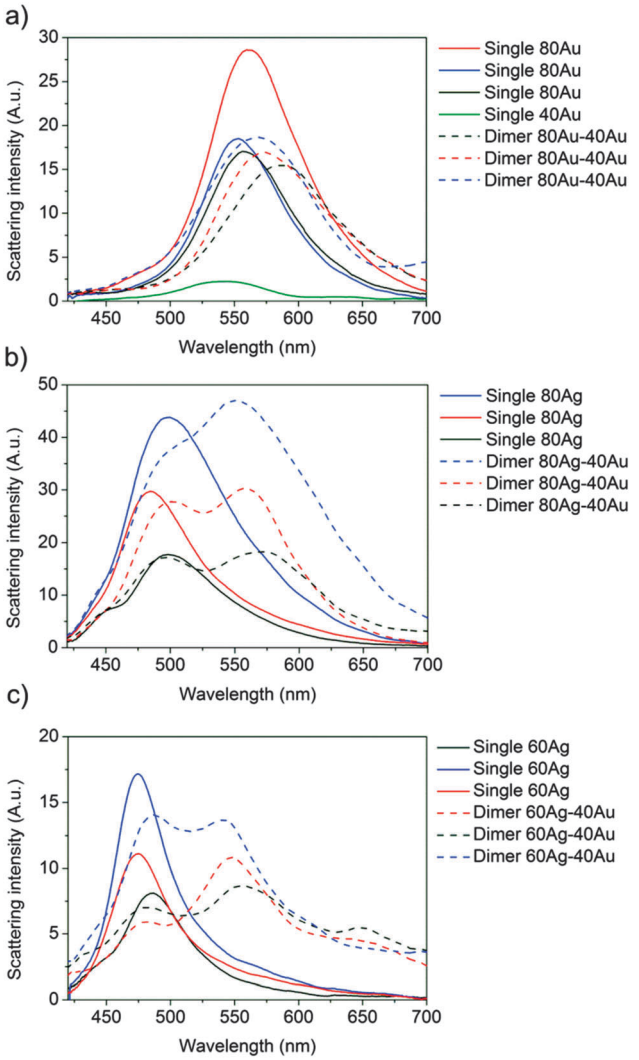

Fig. 4 Smoothed spectroscopic measurements of single (solid) or coupled (dotted) nanoparticles. (a) 80 nm Au–40 nm Au, (b) 80 nm Ag–40 nm Au (c) 60 nm Ag–40 nm Au nanoparticles. The green line in (a) denotes the spectrum of a single 40 nm gold particle. All measurements were made after incubation of the 40 nm AuNPs resulting in a population of singular particles and dimers. See Fig. S5 (ESI†) for raw spectra.

decrease the particle–particle distance and increase the coupling efficiency compared to the 15 nm spacing used in the simulations. For the 80Ag–40Au heterodimers, we see a very large peak appearing around 550 nm, which coincides with the expected red-shifted 40 nm Au peak. The intensity of the 40 nm gold peak shows an even higher intensity enhancement then observed in the simulations. The scattering intensity is a factor of 8 to 20 higher at the plasmon peak wavelength compared to the intensity of a single 40 nm Au particle. The average peak distance between the gold and silver peaks is 65 nm, which is less than the 105 nm observed in the simulations. This can be explained by the red shifted LSPR peaks of the single 80 nm AgNPs, which range from 475 nm to 510 nm, which is about 25 to 50 nm more red shifted than expected. Variations in peak wavelength are anticipated because of the distribution in size and shape of the nanoparticles. A small red shift can, in part, be explained by the salt-buffer environment of the nanoparticles and the DNA layer. However the larger shift is most likely due to a strong interaction between the nanoparticles and the surface, as other researchers have shown similar redshifts for 60 nm silver nanoparticles on glass.[24] The 60Ag–40Au complex gives rise to a much higher relative spectral change compared to that of gold homodimers and slightly better peak separation compared to that of 80Ag–40Au dimers. The average peak-to-peak distance is 70 nm, while the intensity of the 40 nm Au particles is enhanced by a factor of 4 to 7. The Ag–Au complexes show variations in the relative intensities of the gold and silver peaks, which is known to be a function of the polarization angle.[25,26] Since the particles are randomly orientated on the surface, the measured Ag and Au peaks will vary in intensity. In terms of stability of the complexes, the Au–Au dimers showed no apparent change in intensity or color after several days of incubation in salt buffer. However, the Ag–Au complexes displayed a decrease in intensity, together with a redshift and broadening of the silver plasmon peak. We attribute this effect to the oxidation of the silver nanoparticles, which is known to occur.[27] Fortunately, this did not interfere with our measurements, because no changes were detected during the two hours of measurement.

Conclusions

In this paper, we have investigated the plasmonic coupling of nanoparticles for use in (color-based) sensing applications. A figure of merit (FOM) was proposed to relate spectral shifts to shifts in color camera intensity. A higher FOM was obtained for simulated gold nanoparticle homodimers compared to silver homodimers, although silver showed larger peak shifts. The lower FOM for silver is a direct result of the position of the plasmon peak in an area of low sensitivity of the color camera. Heterodimers of large Ag and small Au nanoparticles show high enhancement of the gold plasmon peak, which translates to a much larger FOM compared to homodimers of gold or silver, while the reversed heterodimer composition (large Au, small Ag) showed much weaker plasmon coupling and therefore a smaller spectral shift and FOM. Spectroscopic dark-field measurements performed on individual DNA-coupled nanoparticle dimers show similar spectral shifts as observed for the simulated dimers. Both the small spectral shift of the 80–40 nm gold homodimers, and the larger spectral shifts and gold peak enhancement of the 80–40 Ag–Au and 60–40 Ag–Au dimers are observed. These results indicate that careful selection of size and the use of Au–Ag nanoparticles can significantly increase the spectral response of dimerization events. This can be of use for greatly enhancing the signal of LSPR coupling based color sensors or other dimerization based sensors.[28,29] In turn, this can lead to both improving detection limits and the detection of nanoparticle dimerization at larger inter-particle distances.

Acknowledgements

The authors acknowledge support from the Dutch Technology Foundation STW, project number 11818.

References

1 M. Barreiros dos Santos, J. P. Agusil, B. Prieto-Simón, C. Sporer, V. Teixeira and J. Samitier, *Biosens. Bioelectron.*, 2013, **45**, 174.
2 H. J. Chung, C. M. Castro, H. Im, H. Lee and R. Weissleder, *Nat. Nanotechnol.*, 2013, **8**, 369.
3 J. Zhao, X. Zhang, C. R. Yonzon, A. J. Haes and R. P. Van Duyne, *Nanomedicine*, 2006, **1**(2), 219.
4 H. Wu, J. Henzie, W. Lin, C. Rhodes, Z. Li, E. Sartorel, J. Thorner, P. Yang and J. T. Groves, *Nat. Methods*, 2012, **9**(12), 11.
5 S. Chen, M. Svedendahl, M. Käll, L. Gunnarsson and A. Dmitriev, *Nanotechnology*, 2009, **20**(43), 434015.
6 R. Elghanian, J. J. Storhoff, R. C. Mucic, R. L. Letsinger and C. A. Mirkin, *Science*, 1997, **277**(5329), 1078.
7 A. Jyoti, P. Pandey, S. P. Singh, S. K. Jain and R. Shanker, *J. Nanosci. Nanotechnol.*, 2010, **10**(7), 4154.
8 Y. C. Cao, R. Jin, C. S. Thaxton and C. A. Mirkin, *Talanta*, 2005, **67**(3), 449.
9 R. Verdoold, R. Gill, F. Ungureanu, R. Molenaar and R. P. H. Kooyman, *Biosens. Bioelectron.*, 2011, **27**, 77.
10 L. J. Sherry, S. Chang, G. C. Schatz, R. P. Van Duyne, B. J. Wiley and Y. Xia, *Nano Lett.*, 2005, **5**(10), 2034.
11 J. Zhao, A. O. Pinchuk, J. M. Mcmahon, S. Li, L. K. Ausman, A. L. Atkinson and G. C. Schatz, *Acc. Chem. Res.*, 2008, **41**(12), 1710.
12 C. M. Cobley, S. E. Skrabalak, D. J. Campbell and Y. Xia, *Plasmonics*, 2009, **4**(2), 171.
13 H. Shen, G. Lu, T. Zhang, J. Liu, y. Gu, P. Perriat, M. Martini, O. Tillement and Q. Gong, *Nanotechnology*, 2013, **24**, 285502.
14 N. Nath and A. Chilkoti, *Anal. Chem.*, 2004, **76**(18), 5370.
15 A. D. McFarland and R. P. Van Duyne, *Nano Lett.*, 2003, **3**(8), 1057.
16 H. Chen, X. Kou, Z. Yang, W. Ni and J. Wang, *Langmuir*, 2008, **24**, 5233.
17 C. L. Nehl, H. Liao and J. H. Hafner, *Nano Lett.*, 2006, **6**(4), 683.
18 E. Martinsson, B. Sepulveda, P. Chen, A. Elfwing, B. Liedberg and D. Aili, *Plasmonics*, 2013, **9**(4), 773.
19 X. Zhang, T. Gouriye, K. L. Göeken, M. R. Servos, R. Gill and J. Liu, *Phys. Chem. Chem. Phys.*, 2013, **117**(30), 15677.
20 ICX285AQ CCD factsheet, www.sony.net/Products/SC-HP/datasheet/01/data/E01420B3Z.pdf.
21 J. N. Anker, W. P. Hall, O. Lyandres, N. C. Shah, J. Zhao and R. P. Van Duyne, *Nat. Methods*, 2008, **7**(6), 442.
22 M. Svedendahl, S. Chen, A. Dmitriev and M. Käll, *Nano Lett.*, 2009, **9**(12), 4428–4430.
23 J. H. Yoon, Y. Zhou, M. G. Blaber, G. C. Schatz and S. Yoon, *J. Phys. Chem. Lett.*, 2013, **4**, 1371.
24 M. Hu, A. Ghoshal, M. Marquez and P. G. Kik, *J. Phys. Chem. C*, 2010, **114**, 7509.
25 F. Chen, N. Alemu and R. L. Johnston, *AIP Adv.*, 2011, **1**(3), 032134.
26 S. Sheikholeslami, Y. Jun, P. K. Jain and A. Alivisatos, *Nano Lett.*, 2010, **10**(7), 2655.
27 Y. Han, R. Lupitskyy, T.-M. Chou, C. M. Stafford, H. Du and S. Sukhishvili, *Anal. Chem.*, 2011, **83**(15), 5873.
28 K. E. Fong and L.-Y. L. Yung, *RSC Adv.*, 2012, **2**, 5154.
29 W. P. Hall, S. N. Ngatia and R. P. Van Duyne, *J. Phys. Chem. C*, 2011, **115**(5), 1410.